Characteristics of a Pair of Small Field-of-View LSO Scintillation Cameras

J. Seidel[a], W. R. Gandler[b] and M. V. Green[a]
[a]Nuclear Medicine Department, National Institutes of Health, Bethesda, MD 20892, USA
[b]Division of Computer Research and Technology, National Institutes of Health, Bethesda, MD 20892, USA

ABSTRACT

We created two miniature scintillation cameras by coupling identical, thin LSO crystals to position sensitive photomultiplier tubes (PSPMTs). The performance of these cameras was established in both single photon and coincidence imaging modes and in relation to similar gamma cameras equipped with NaI(Tl) crystals. The intrinsic spatial resolution of the LSO cameras was 2.3 mm at 140 keV and 1.2 mm at 511 keV. The coincidence time resolution was 3 ns with an energy resolution of 16.5% at 511 keV. With no sources present, an intrinsic event rate of 300/sec/cm^3 of LSO from ^{176}Lu was observed. Although this background count rate may be a limitation in some applications, LSO PSPMT scintillation cameras offer several important performance advantages over similar NaI(Tl) and BGO cameras that include improved count rate performance, coincidence timing, stopping power relative to NaI, and energy resolution relative to BGO.

I. INTRODUCTION

Small field-of-view, position-sensitive photomultiplier tube (PSPMT) cameras have a variety of potential applications ranging from small animal imaging to imaging selected parts of the human body. Limitations encountered in these applications could, in principle, be minimized or eliminated by replacing NaI(Tl) or BGO with a Lutetium-based scintillator such as the recently proposed [1-3] $Lu_2(SiO_4)O$:Ce or LSO. We sought to test this conjecture experimentally by (1) measuring the physical properties of LSO and (2) by evaluating the coincidence and single photon imaging characteristics of this material when coupled to a pair of PSPMTs.

II. EXPERIMENTS AND RESULTS

A. Physical Characteristics of LSO

Two thin, unfinished disks of LSO were kindly provided by Schlumberger-Doll Research. After geometric regularization and polishing, visual inspection revealed crystals with a slight tint and with microscopic, reflective inclusions distributed homogeneously throughout the material. Physical measurements made on these crystals are listed in Table I, including the (narrow beam) linear attenuation coefficient, μ, of LSO at 140 keV (^{99m}Tc) and 511 keV (^{18}F).

Table I. Physical characteristics of the LSO crystals

diameter	23.7 mm
depth	4.7 mm
weight	15.4 g
density	7.4 g/cm^3
μ at 140 keV	9.6 cm^{-1}
μ at 511 keV	0.86 cm^{-1}

An additional physical property of Lu is the radioactivity of the 2.6% abundant isotope ^{176}Lu. The energy spectrum of gamma rays escaping from the LSO crystals, recorded with a standard 1.5" x 1.5" NaI(Tl) detector, is shown in Figure 1. Peaks are evident near 300, 200 and 60 keV, corresponding closely to the known γ-ray and x-ray emissions of ^{176}Lu [3]: 306, 202 keV γ-rays, Hf K x-rays (K_α 55 keV, K_β 63 keV).

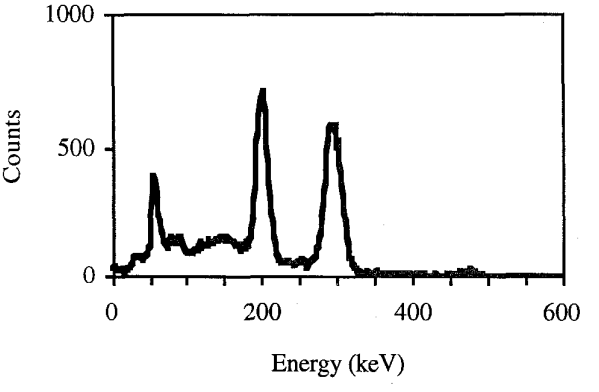

Fig. 1 Extrinsic emission spectrum of LSO measured with a NaI(Tl) detector.

B. Scintillation Camera Setup

Before coupling the crystals to the PSPMTs, all surfaces but the exit surface were painted flat black. This surface treatment was used to optimize spatial resolution but is suboptimal for energy and time resolution. The two crystals were then coupled with optical grease to two 3" square PSPMTs (Hamamatsu R3941) to form two identical small-field-of-view scintillation cameras. The X,Y location of a scintillation event

was determined by resistive charge division. Standard wideband preamplifiers (Philips 771) and shaping amplifiers (EG&G 835) with a 0.5 μs time constant were used to amplify the four position signals (2 for X, 2 for Y) from each PSPMT. The energy (total charge) associated with the scintillation event was obtained from the sum of the position signals. The time information of an event was derived from the signal of the PSPMT's last dynode, which was inverted, amplified (EG&G FTA820) and fed into a constant fraction discriminator (CFD). The coincidence time spread function was measured with a time-to-amplitude converter (EG&G 567), whose start and stop inputs were triggered by the two cameras' CFD signals.

C. Energy Spectra and Scintillation Linearity

In order to estimate the internal disintegration rate of ^{176}Lu in these LSO cameras, the energy threshold of each camera was set near zero. With no external sources present, the total, intrinsic event rate within each crystal was 300 cps/cm^3 (or 40 cps/g) of LSO.

Energy spectra obtained with the cameras, due to ^{176}Lu (or to external radiation sources), were acquired from a 2 mm x 2 mm region located at the center of each crystal. The intrinsic spectrum of the ^{176}Lu decay, recorded from this central region with no external sources present, is shown in Figure 2. The count rate in a 200 keV wide window centered at 511 keV was one-third of the total counts in the spectrum, or 100 cps/cm^3, whereas for a 80 keV window centered at 140 keV, it was 5% of the total, or 15 cps/cm^3.

Energy spectra from external sources of ^{99m}Tc, ^{67}Ga, ^{18}F and ^{137}Cs were also obtained. The ^{18}F spectrum is shown in Figure 3. The relative energy resolution for the 511 keV photopeak was $\Delta E_{FWHM}/E$ = 16.5%. In these experiments, the count rate from the isotopic sources was always much greater than the intrinsic rate from ^{176}Lu so that contamination of the isotopic spectra by ^{176}Lu was negligible.

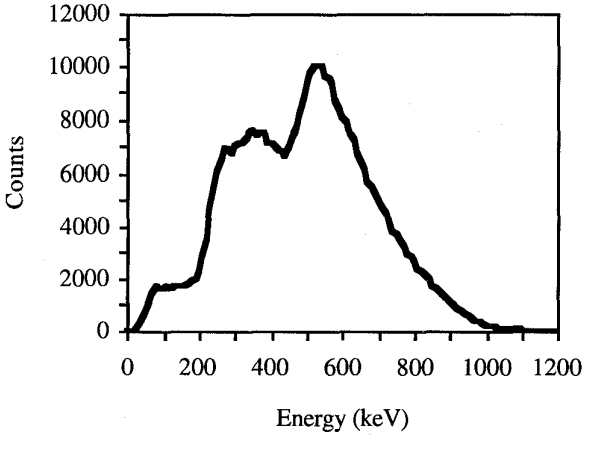

Fig. 2 Intrinsic LSO energy spectrum seen by PSPMT.

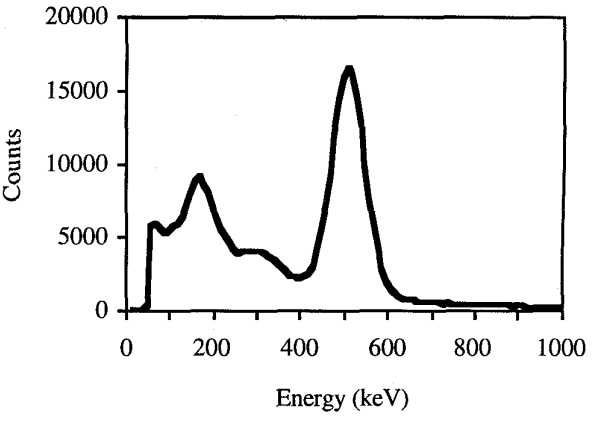

Fig. 3 ^{18}F energy spectrum measured with PSPMT.

These energy spectra were analyzed to determine the differential nonlinearity (DNL) of LSO's scintillation efficiency with photon energy (cf. Ref. [5]). DNL was calculated with the expression:

$$DNL = const * (P2-P1) / (E2-E1),$$

where P1, P2 are the locations of photopeaks with neighboring energies E1, E2. DNL for LSO is plotted against energy in Figure 4. The data are normalized to a value of 1 at the highest energy.

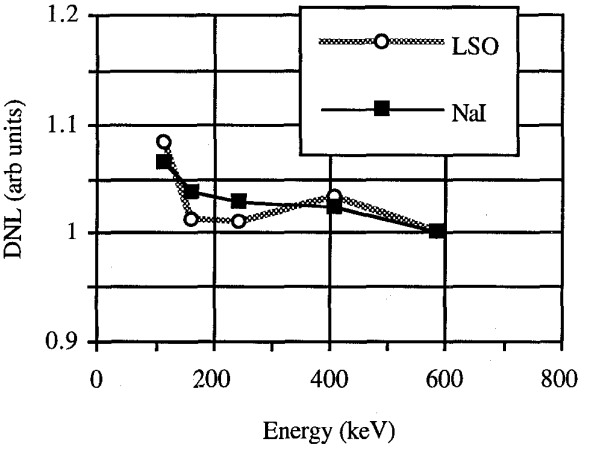

Fig. 4 Differential nonlinearity of LSO and NaI(Tl) scintillation efficiency.

D. Spatial Linearity

An important limitation of the LSO scintillation minicameras arises from the small crystal size. Edge effects distort the light collection process appreciably so that the centroid of the light distribution no longer represents the true location of the scintillation event. Events occurring in the outer 5-6 mm wide rim tend to be positioned in a narrow ring.

This effect is evident in the ^{18}F field flood image shown in Figure 5. As a result of these edge distortions, only the central region, appearing in Fig. 5 as a dark circle 10-12 mm in diameter, shows a linear response in spatial positioning. This inner, linear region is, however, large compared to the observed widths of the point spread functions. Since the crystals were always illuminated at their centers, spatial resolution measurements should be unaffected by edge distortions.

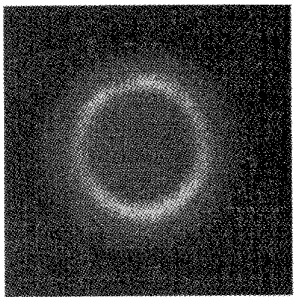

Fig. 5 Field flood image acquired with ^{18}F.

E. Spatial Resolution

The intrinsic spatial resolution of the LSO minicameras was determined for incident 140 and 511 keV photons. A 5 cm thick Pb brick with a central 2 mm diameter hole was used to collimate the incident single photon beams. An image of the hole for a ^{99m}Tc source is shown in Figure 6. The width of the 140 keV point spread function obtained from Fig. 6 was FWHM = 2.3 mm after corrections for hole diameter and source size.

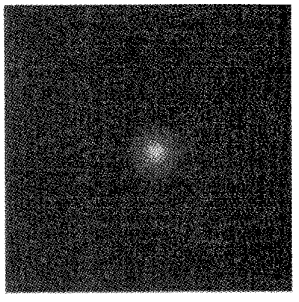

Fig. 6 Image of collimated ^{99m}Tc source.

At 511 keV, two effects were observed that compromised the single photon measurement of spatial resolution. First, the projected image of the hole was superimposed on the radiation background from ^{176}Lu (Figure 7A) and second, the measured width of the point spread function was found to be nearly equal to the hole diameter, implying a camera resolution much smaller than the hole size.

As a result, the coincidence setup shown in Fig. 8 was employed to obtain a more accurate estimate of intrinsic spatial resolution at 511 keV. In this arrangement the ^{176}Lu background was first eliminated by placing the detectors in time coincidence. The hole size effect was then minimized by exploiting a favorable geometry and by utilizing the fact that the annihilation gamma rays are nearly collinear. In this configuration, the source was placed very near one detector. Radiation from this source was collimated and allowed to fall on the second, more distant detector. In this geometry, coincidence lines connecting the two detectors through the collimator and the source will "paint" a small image of the source on the closer detector (the PSPMT camera on the left in Figure 8). In contrast to single photon illumination, however, the size of this painted image will be dominated by the smaller (1.1 mm) size of the source rather than the larger (2 mm) size of the hole. An image of the source formed on the left PSPMT camera using this coincidence setup is shown in Figure 7B. After correcting the apparent size of this spot for the source size, the FWHM of the point spread function, or intrinsic spatial resolution of the detector at 511 keV, was estimated to be 1.2 mm.

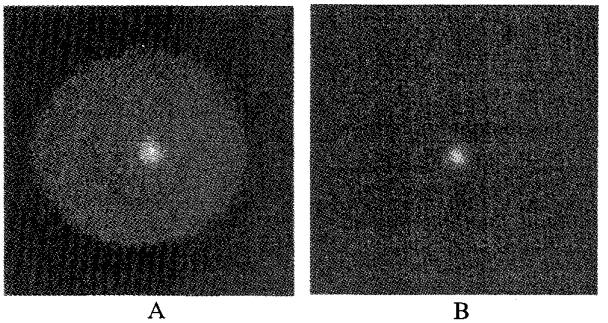

Fig. 7 Point source images at 511 keV obtained in single photon (A) and coincidence modes (B).

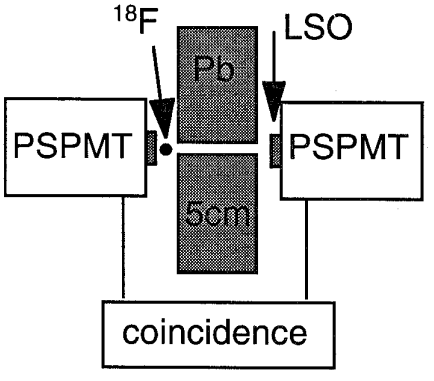

Fig. 8 Coincidence setup used in measuring intrinsic spatial resolution at 511 keV.

F. Time Resolution

Coincidence time resolution was measured as described in part II.B. Time resolution, defined as the FWHM of the time-to-amplitude converter spectrum, was 3 ns using an energy threshold of approximately 200 keV for events in each detector.

G. Measurements with NaI(Tl)

After the LSO measurements were completed, the LSO disks were removed from the PSPMTs and replaced with continuous slabs of NaI(Tl) that covered the effective field-of-view of each PSPMT (approximately 60 mm x 50 mm). After modification of the electronics to accommodate NaI(Tl), a subset of the LSO measurements were repeated with these NaI(Tl) minicameras. LSO and NaI(Tl) results are compared in Table II. Differential nonlinearity of NaI(Tl) is graphically portrayed in Figure 4.

Table II. Comparison of characteristics of PSPMT scintillation cameras with thin LSO and NaI(Tl) crystals

	LSO	NaI(Tl)
thickness	4.7 mm	4 mm
spatial FWHM, 140 keV	2.3 mm	1.6 mm
spatial FWHM, 511 keV	1.2 mm	0.95 mm
$\Delta E_{FWHM}/E$ at 511 keV	16.5%	9.6%
time resolution (200 keV threshold).	3 ns	9 ns

III. DISCUSSION

Continuous crystal, small field-of-view PSPMT scintillation cameras have found many applications in both human and small animal imaging [6-11]. Generically, the performance of these devices can be enhanced by increasing the stopping power of the scintillator (to increase sensitivity), by increasing the amount and the efficiency of collection of fluorescent light released during a scintillation (to increase spatial and energy resolution), by reducing crystal thickness, (to reduce image distortion and increase spatial resolution) and by reducing the scintillation decay time (to increase count rate performance). The results listed in Tables I-II indicate that LSO possesses many of these desirable properties relative to NaI(Tl): the linear attenuation coefficient of LSO is 4 times greater than NaI(Tl) at 140 keV and 2.6 times greater at 511 keV; spatial resolution, though relatively poorer than for NaI(Tl), is still acceptable, and time resolution is at least a factor of three better than that for NaI(Tl). In addition, the reported LSO light decay time [1,2] of 42 nsec is more than a factor of 6 shorter than that reported for NaI(Tl) [2]. Finally, LSO and NaI(Tl) exhibit similar, modest variations in scintillation efficiency with photon energy over the photon energy range examined in this study.

In order to provide independent corroboration for some of the measurements listed in Table I, and to allow comparison of LSO with BGO, we calculated the theoretical linear attenuation coefficients at 140 and 511 keV, and photofractions at 511 keV, of LSO, NaI(Tl) and BGO. These values are listed in Table III. As expected, at low energies LSO and BGO both possess very large linear attenuation coefficients compared to NaI(Tl). At 511 keV, the linear attenuation coefficient of LSO is about 90% and the photofraction about 75% those of BGO. The stopping power of LSO is, therefore, somewhat less than for BGO at this energy. However, the timing advantages of LSO relative to BGO are even greater than for NaI(Tl): the decay time of the LSO light pulse is nearly 8 times shorter than that of BGO [2] so that much higher count rates should be attainable with LSO. This gain in count rate capability would appear largely to offset the slight reduction in stopping power of LSO compared to BGO.

Table III. Linear attenuation coefficient μ, in cm^{-1}, and photofraction ϕ, for three scintillators. Data were obtained using the tables of Ref. [12].

	NaI	LSO	BGO
μ at 140 keV	2.4	9.7	12.1
μ at 511 keV	0.33	0.86	0.95
ϕ at 511 keV	0.18	0.33	0.41

Although LSO has been most often mentioned as a candidate to replace BGO in PET applications, the results obtained in this study suggest that LSO PSPMT cameras may also offer performance advantages in the low energy, single photon imaging mode compared to NaI(Tl) scintillation cameras. For example, 86% of incoming 140 keV photons would interact in a 2 mm thick LSO crystal, compared to 76% in a 6 mm thick NaI(Tl) crystal, and a greater fraction of these events would be total absorptions. An LSO camera with a 2 mm thick crystal would be expected to have a spatial resolution appreciably better than the 2.3 mm measured here, perhaps approaching that of the 4 mm thick NaI(Tl) camera, while at the same time being capable of counting at much higher rates. This combination of advantages in sensitivity, resolution and count rate would be very useful in high count rate studies such as first-pass cardiac imaging in small animals.

Continuous crystal, LSO PSPMT cameras also offer advantages over BGO in PET or positron imaging. For example, if the continuous slab crystals in a BGO-based (coincidence) projection imaging system [11] were replaced with LSO, higher resolution images should be obtained (because of the higher scintillation efficiency of LSO) at higher count rates (shorter light pulses) and with little reduction in sensitivity (Table III) compared to BGO. Similarly, a NaI(Tl)-based, very high resolution, single slice small animal PET scanner [10] would exhibit a much higher detection sensitivity (greater stopping power at 511 keV) with relatively little loss in spatial resolution (Table II) if the NaI(Tl) were replaced with LSO. Both of these devices, whose applications include projection imaging of the human female breast, whole body imaging of small animals, and

tomographic imaging of small animal organs, would exhibit improved performance with LSO.

Several disadvantages of LSO can be identified: (1) the ^{176}Lu background, (2) a lower light output than NaI(Tl) and (3), the unavailability of LSO in large area, continuous slabs sufficient to cover the useful area of a conventional PSPMT (about 65 mm x 55 mm = 35.75 cm^2).

The magnitude of the Lu background for various cameras can be estimated. For example, a PSPMT coupled to a 2 mm thick slab of LSO covering the field-of-view would exhibit a total count rate of 300 cps/cm^3 x 35.75 cm^2 x 0.2 cm = 2145 cps due to this background. This count rate would be superimposed on whatever count rate was occurring due to external sources. In addition, an image of the crystal would also be superimposed on the image of whatever external object was being imaged (as in Figure 7A). The relative importance of this "background image" depends on the relative strength of the background and the object as "seen" in the energy window set to image the object. If this window is located in the vicinity of 140 keV (see Figure 2), background contamination would be minimal. On the other hand, if the energy window is set near the 511 keV annihilation photopeak, the background rate would be higher. Although an absolute background rate of a few hundred, or even a few thousand counts per second, does not pose a particularly difficult technical problem, the presence of this background could complicate imaging and quantification of weak single photon sources. Thicker crystals of LSO, as would be required in the BGO (coincidence) projection imaging system [11], would exhibit an even greater background rate. If the BGO crystals in this system were replaced with LSO, the total background rate would be nearer to 15,000 cps in each camera rather than 2000 cps. Fortunately, in the coincidence mode of operation, the high count rate capability and coincidence timing properties of LSO would essentially eliminate this background effect (as in Figure 7B).

Although the Lu background introduces a greater or lesser source of "noise" into the imaging process, this very long-lived, homogeneously distributed background can also serve a useful purpose by acting as a permanent, built-in "field flood" source. This internal source could be used to quantify and correct non-uniformities in the imaging field and to quantify long-term system stability. Another effect of this Lu background is also observable under certain circumstances: two LSO PSPMT cameras with crystals in close proximity, and in time coincidence, will exhibit a true coincidence rate even when no sources are present. The observed rate depends strongly on detector separation and on energy window in each detector. Coincidence events occur when a gamma ray or x-ray escapes from one detector and is absorbed in the other, while in the first detector a simultaneous signal is generated by internal absorption of the beta particle or other radiations emitted in the decay of ^{176}Lu.

A second disadvantage of LSO is that it exhibits a scintillation efficiency less than NaI(Tl). In PSPMT cameras, where the accuracy of event positioning depends largely on scintillator efficiency, less light generally translates into poorer spatial (and energy) resolution. The results shown in Table II confirm this effect. Although these measurements were not made with the purpose of estimating relative light output, and are not rigorously comparable, they are consistent with a relative light output for LSO that is roughly 55-60% that of NaI(Tl), a value similar to the 50% found in Ref. [3], but somewhat lower than reported elsewhere (75% in Ref. [1]). Despite this difference, however, the absolute spatial resolution differences between LSO and NaI(Tl) are small, particularly at 511 keV. Scatter rejection will also be poorer with LSO because of this effect, though this reduction seems acceptable given the substantial improvements in stopping power and timing relative to NaI(Tl).

Finally, a practical disadvantage exists with LSO: LSO is not now commercially available in single crystals with cross-sectional areas comparable to the field-of-view of contemporary PSPMTs. Commercialization of this material is, however, reportedly underway and material suitable for making pixellated detectors should be available shortly. Thus, some of the advantages noted here may be first demonstrated with pixellated PSPMT [13,14] cameras. Larger area, single crystals of LSO, although more difficult to produce, would be expected to follow if these initial efforts prove successful.

IV. CONCLUSION

Small field-of-view PSPMT scintillation cameras made with LSO should exhibit several significant performance advantages over cameras made with NaI(Tl) and BGO in the photon energy range associated with positron and single photon imaging studies. These advantages are such that LSO, if available, could well replace these materials in many applications, while stimulating new detector designs that capitalize on these properties.

V. REFERENCES

[1] C. L. Melcher and J. S. Schweitzer, "Cerium-doped Lutetium Oxyorthosilicate: A Fast, Efficient New Scintillator," *IEEE Trans Nucl Sci,* Vol. 39, pp. 502-505, 1992

[2] F. Daghighian, P. Shenderov, K. S. Pentlow, M. C. Graham, B. Eshaghian, C. L. Melcher, J. S. Schweitzer, "Evaluation of Cerium Doped Lutetium Oxyorthosilicate (LSO) Scintillation Crystal for PET," *IEEE Trans Nucl Sci*, Vol. 40, pp. 1045-1047, 1993

[3] T. Ludziejewski, K. Moszynska, M. Moszynski, D. Wolski, W. Klamra, L. O. Norlin, W. Devitsin, V. Kozlov, "Advantages and Limitations of LSO Scintillator in Nuclear Physics Experiments," *IEEE Trans Nucl Sci,* Vol. 42, pp. 328-336, 1995

[4] C. M. Lederer and V. S. Shirley, eds., "Table of Isotopes," 7th ed., Wiley Interscience, New York, 1978

[5] G. F. Knoll, *Radiation Detection and Measurement,* 2nd ed., New York: John Wiley & Sons, 1989

[6] M. V. Green, M. P. Andrich, D. Doudet, A. Markowitz, T. E. Tedder, E. S. Owens, M. I. Chaparro and R. D. Neumann, "Evaluation of Cardiovascular Function in Small Animals Using a Microcomputer-based Scintigraphic Imaging System," *Proceedings of Computers in Cardiology 1991,* Venice, Italy, IEEE Computer Society Press, pp. 233-236, 1992

[7] M. V. Green, A. Markowitz, T. E. Tedder, M. P. Andrich, E. S. Owens and R. D. Neumann, "SPECT Imaging in Small Animals," *J Nucl Med,* Vol. 33, 852P, 1992

[8] N. J. Yasillo, J. N. Aarsvold, R. N. Beck, T. A. Block, C.-T. Chen, M. Cooper, S. J. Heimsath, K. L. Matthews, R. A.

Mintzer, X. Pan, T. C. Vazquez, C. Wu, "A Clinical Miniature Gamma Camera," *J Nucl Med,* Vol. 34, 112P, 1993

[9] Z. He, A. J. Bird, D. Ramsden, Y. Meng, " A 5 Inch Diameter Position-Sensitive Scintillation Counter," *IEEE Trans Nucl Sci,* Vol. 40, pp. 447-451, 1993

[10] J. Seidel, W. R. Gandler, M. V. Green, "A Very High-Resolution Single-Slice Small Animal PET Scanner Based on Direct Detection of Coincidence Line Endpoints," *J Nucl Med,* Vol. 35, 40P, 1994

[11] J. Seidel, W. R. Gandler, I. N. Weinberg, A. Markowitz, N. J. Lobaugh, and M. V. Green, "Collimatorless Projection Imaging of Positron Emitters with an Opposed Pair of BGO Scintillation Cameras," *J Nucl Med,* Vol. 36, 177P, 1995

[12] E. F. Plechaty, D. E. Cullen, R. J. Howerton, "Tables and Graphs of Photon-Interaction Cross Sections from 0.1 keV to 100 MeV derived from the LLL evaluated-Nuclear-Data Library," Report UCRL-50400, Vol. 6, Rev. 2, 1978

[13] C. J. Thompson, K. Murthy, I. N. Weinberg, F. Mako, "Feasibility Study for Positron Emission Mammography," *Med Phys,* Vol. 21, pp. 529-537, 1994

[14] M. Watanabe, T. Omura, H. Kyushima, Y. Hasegawa and T. Yamashita, "A Compact Position-Sensitive Detector for PET," *IEEE Trans Nucl Sci,* Vol. 42, pp. 1090-1094, 1995